metals

MDPI

Article

Research on Fatigue Life Prediction Method of Key Component of Turning Mechanism Based on Improved TCD

Tingting Wang, Han Zhang, Yuechen Duan, Mengjian Wang and Dongchen Qin *

School of Mechanical and Power Engineering, Zhengzhou University, Zhengzhou 450000, China; wangtingting@zzu.edu.cn (T.W.); zhanghan2019901@163.com (H.Z.); duanyc1984@zzu.edu.cn (Y.D.); wangmengjian@gs.zzu.edu.cn (M.W.)

* Correspondence: dcqin@zzu.edu.cn; Tel.: +86-2386-8575

Abstract: The main objective of this paper is to accurately obtain fatigue life prediction for the key components of a turning mechanism using the improved theory of critical distances (TCD). The irregularly shaped rotating arm is the central stressed part of the turning mechanism, which contains notches. It has been found that TCD achieves good results in predicting the fatigue strength or fatigue life of notched components with regular shape but is less commonly used for notched components with irregular shape. Therefore, TCD was improved and applied broadly to predict the fatigue life of an irregularly shaped rotating arm. Firstly, the notch depth and structure net width parameters were introduced into the low-order and low-accuracy classical TCD function to obtain a novel stress function with high computational efficiency and high accuracy, whereas the stress concentration factor was introduced to modify the length of critical distance. Secondly, the improved TCD was used to predict the fatigue strength of notched components with regular shape, and its accuracy was demonstrated by a fatigue experiment. Finally, the improved TCD was applied to predict the fatigue life of an irregularly shaped rotating arm. The deviation between prediction results and experimental results is less than 18%. The results demonstrate that the improved TCD can be applied effectively and accurately to predict the fatigue life of key components of turning mechanisms.

Keywords: rotating arm; fatigue life prediction; theory of critical distances; stress function; critical distance length; fatigue experiment

Citation: Wang, T.; Zhang, H.; Duan, Y.; Wang, M.; Qin, D. Research on Fatigue Life Prediction Method of Key Component of Turning Mechanism Based on Improved TCD. *Metals* **2022**, *12*, 506. https://doi.org/10.3390/met12030506

Academic Editors: Alberto Campagnolo and Giovanni Meneghetti

Received: 12 January 2022
Accepted: 14 March 2022
Published: 16 March 2022

1. Introduction

As the kernel component of garbage compression trucks, the primary function of the turning mechanism is to lift and frequently turn over trash cans to dump trash into the carriage. This mechanism is subjected to alternating tensile loads, resulting in fatigue damage, which affects the regular use of the garbage compression truck. Therefore, it is crucial to accurately predict the fatigue life of key components of the turning mechanism to ensure the reliability of garbage compression trucks.

Fatigue life analysis of the turning mechanism of garbage compression trucks is often carried out using the nominal stress method [1–5]. The method is simple to apply but leads to inaccurate prediction because it does not take into account the influence of the stress field around the notch. Considering the above problems, in the 1950s, Neuber and Peterson [6,7] proposed the theory of critical distances. The theory suggests that the fatigue failure of notched components is not only determined by the maximum stress at the notch but is also affected by the stress field near the notch. Based on this theory, many scholars have predicted the fatigue performance of notched components under different conditions and have achieved good results [8–13]. In the application of conventional TCD, an accurate description of the stress field around the notch is essential for predicting the results. The stress field around the notch was first calculated using the complex variable function. Still, it was later found that it was difficult to obtain an analytical solution using this method,

and many approximate expressions were proposed, with the most commonly used being the stress functions proposed by Glinka et al. [14–18]. Among these functions, those of low order are computationally efficient but not very accurate, whereas those of high order are more accurate but less efficient. In addition, the length of the critical distance is also significant in the application of TCD. The length of the critical distance is usually considered a constant that depends entirely on the properties of the material. However, it has been found [19,20] that in practice, the length of the critical distance depends on the properties of the material but is also influenced by the structure. For this reason, several corresponding compensating methods have been proposed to modify the length of the critical distance. Taddessen [21] combined the concept of cyclic plastic zone (CPZ) to propose a new method for calculating the length of critical distance, and the method has higher accuracy compared to the classical TCD and the Susmel and Taylor models. Yang et al. [22] found a close relationship between critical distance, linear elastic stress concentration factor and fracture life. Wang et al. [23] studied the influence of the statistical size of the bolt hole on low-cycle fatigue life and proposed a method that combined critical distance with the high-stress volume model. Sun et al. [24] proposed a new modification method based on the relative stress gradient to determine the length of the critical distance of a crankshaft in order to predict the fatigue limit load. Comparison between the prediction and the experimental results showed that this new modified approach could provide a more satisfactory result than the traditional TCD. Because TCD is effective in assessing the fatigue performance of notched components, more and more scholars are applying the theory to engineering practice and supplementing and refining the theory. Considering the inhomogeneity of stress distribution near the notch, Moritz and Shen et al. [25,26] introduced stress gradients into traditional TCD. Wang and Li et al. [27,28] introduced the weight function of the relative stress gradient into the traditional TCD; they used this method to successfully predict the low-cycle fatigue life of TA19 notched specimens. TCD was initially used to predict the high-cycle fatigue strength of notched components under uniaxial loading. Later, Susmel and Taylor et al. [29,30] extended the TCD to multiaxial fatigue loading. In recent years, many scholars have put more focus on this area. Bowen et al. [31] comprehensively considered the influence of axial and torsional loads on notch fatigue life and introduced a new multiaxial notch parameter based on the critical distance–fatigue life curves of the two loads, and the method was experimentally proven to be consistent with the modified Wöhler curve method (MWCM) in planar fatigue assessment. Benedetti [32] combined TCD with a multiaxial fatigue criterion for predicting the fatigue strength of notched components, and the method can predict the fatigue life of notched components with residual stresses. Nicholas Gates [33] also applied the method to a multiaxial fatigue criterion and took other factors, such as the stress gradient and notch root radius, into account. Comparison between the prediction and the experimental results showed that the method had greater accuracy in practical applications than traditional fatigue analysis methods. The application of TCD for multiaxis loading is not yet well established and still needs to be investigated in more depth in the future. TCD is a particular local fatigue analysis method. Other local fatigue methods [34,35] have been studied in the past and used to analyze the details of materials and structures in fatigue. However, TCD may be more widely used than other local fatigue analysis methods.

As seen from current studies, whether for uniaxial or multiaxial loads, TCD is mostly applied for notched components with regular shape and less for notched components with irregular shape. In this paper, we investigate the application of TCD for key components of the turning mechanism with irregular shapes. The fitting accuracy of the stress function in classical TCD is not high, and the critical distance length is often considered to be related to material properties only, without considering the influence of structural dimensions, thus affecting the accuracy of the prediction results. To improve the fatigue life prediction accuracy of key components of the turning mechanism, in this paper, we improved the TCD in terms of both the stress function and the critical distance length. We verified the effectiveness of the improved TCD through simulation and test comparison. The improved

TCD was then applied to fatigue life prediction of the rotating arm and was found to have a high prediction accuracy. In Section 2, we introduce notch depth and structure net width parameters to the classical stress function to obtain a novel stress function with high computational efficiency and accuracy, as well as a stress concentration factor to modify the critical distance length. In Section 3, we present the simulation and experimental verification. Section 4 deals with fatigue life prediction of the rotating arm. In Section 5, we summarize the main conclusions.

2. Materials and Methods

2.1. Theory of Critical Distances

Theory of critical distances (TCD) takes the overall stress distribution near the notch as the key factor affecting the failure of materials or structures. It is considered that when the average stress in a specific area near the notch exceeds the fatigue strength, fatigue failure of materials or structures will occur. TCD can be summarized as point method, line method, surface method, and volume method. Among them, the point method and line methods [36] are the most widely used. The principle is as follows:

(1) Point Method (PM)

The stress at a point with a certain distance from the notch root is used as the effective stress to predict the fatigue performance of structural components. This distance is defined as $L_0/2$, as shown in Equation (1).

$$\sigma_{eff} = \sigma(x)\big|_{x=L_0/2} \tag{1}$$

where σ_{eff} is the effective stress, L_0 is the material characteristic length, and $\sigma(x)$ is the stress function on the focusing path.

(2) Line Method (LM)

The average stress within a certain distance from the notch root is taken as the effective stress to predict the fatigue performance of structural components. This distance is defined as $2L_0$, as shown in Equation (2).

$$\sigma_{eff} = \frac{1}{2L_0}\int_0^{2L_0} \sigma(x)dx \tag{2}$$

A schematic diagram of the point method and line method is shown in Figure 1.

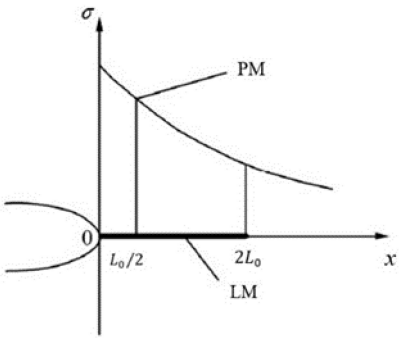

Figure 1. Schematic diagram of point method and line method.

From the principles of TCD, the description of the notched stress field and the selection of critical distance are crucial to the prediction results of notched components. Therefore, the next part of this paper will be an in-depth study of these two aspects.

2.2. Improved Theory of Critical Distances

2.2.1. Presentation of Novel Stress Function

The stress field near the notch is generally described by an approximate expression. Initially, the stress Functions (3)~(5) proposed by Glinka [14], Kujanski [15] and Filippi [16] were often used to approximately describe the stress field near the notch. Later, considering the complexity of the actual structure, some scholars [17,18] proposed higher-precision Functions (6) and (7):

$$\sigma(x) = \frac{\sigma_{\max}}{3}\left[1 + \frac{1}{2}\left(1 + \frac{x}{R}\right)^{-2} + \frac{3}{2}\left(1 + \frac{x}{R}\right)^{-4}\right] \tag{3}$$

$$\sigma(x) = \frac{\sigma_{\max}}{2}\left[\frac{1}{2}\left[\left(1 + \frac{2x}{R}\right)^{-0.5} + \left(1 + \frac{2x}{R}\right)^{-1.5}\right] + \left(1 + \frac{8x}{R}\right)^{-0.5}\right] \tag{4}$$

$$\sigma(x) = \sigma_{\max}\left[1 - 2.33\left(\frac{x}{R}\right) + 2.59\left(\frac{x}{R}\right)^{1.5} - 0.907\left(\frac{x}{R}\right)^{2} + 0.037\left(\frac{x}{R}\right)^{3}\right] \tag{5}$$

$$\sigma(x) = \sigma_{\max}\left[1 + a_1\left(\frac{x}{R}\right) + a_2\left(\frac{x}{R}\right)^{2} + a_3\left(\frac{x}{R}\right)^{3} + a_4\left(\frac{x}{R}\right)^{4}\right] \tag{6}$$

$$\sigma(x) = \sigma_{\max}\left[a_1 + a_2\left(\frac{R}{R+x}\right) + a_3\left(\frac{R}{R+x}\right)^{2} + a_4\left(\frac{R}{R+x}\right)^{3} + a_5\left(\frac{R}{R+x}\right)^{4}\right] \tag{7}$$

where $\sigma(x)$ is the stress function on the focusing path, σ_{max} is the maximum stress, x is the distance from the notch root, R is the notch radius, and a_1~a_5 are fitting coefficients.

Among the above functions, Functions (3)~(5) are only applicable to some circular gaps and less applicable to other types of gaps. Although Functions (6) and (7) have a wide range of applications, their computational effort increases accordingly. Based on the above problems, a new function with high fitting accuracy and less calculation is proposed. It is found that in addition to the notch radius, other dimensions of the structure also affect the stress field near the notch [37]. Therefore, in this paper, we takes a simple structural component as an example and first investigate the influence of important structural dimensional parameters on the stress field near the notch to prepare for the proposed new function.

As shown in Figure 2, it is a plate with two side notches; the parameters B, b, H, R, and L are the total width, net width, notch depth, notch radius, and length of the plate, respectively, and the influence of the plate thickness is not considered. The notch depth, H, and notch radius, R, are the main parameters controlling the notch shape in practical application. A large amount of literature has shown that the notch radius, R, has an important effect on the stress field; this parameter is not discussed here. In addition, parameters B and b both denote the width of the plate, and they have a linear correlation. It should also be noted that the notch depth, H, is the geometric parameter that controls the shape of the notch; the net width, b, is the geometric parameter that controls the shape of the structure; and they are independent parameters. In summary, in this paper, we explore the effects of b, H, and L on the stress field near the notch.

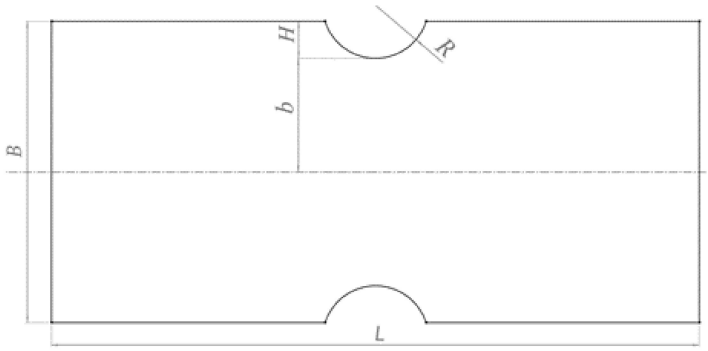

Figure 2. A plate with two side notches.

Considering the constraints and test conditions, finite element simulation is used to obtain the stress–distance curve on a specified path near the notch, and then the effect of changes in b, H, and L on the stress is analyzed. The stress mentioned above is equivalent stress, also known as von Mises stress. This value is defined by the fourth strength theory and comprehensively considers the influence of the first, second, and third principal stresses. The results are shown in Figure 3.

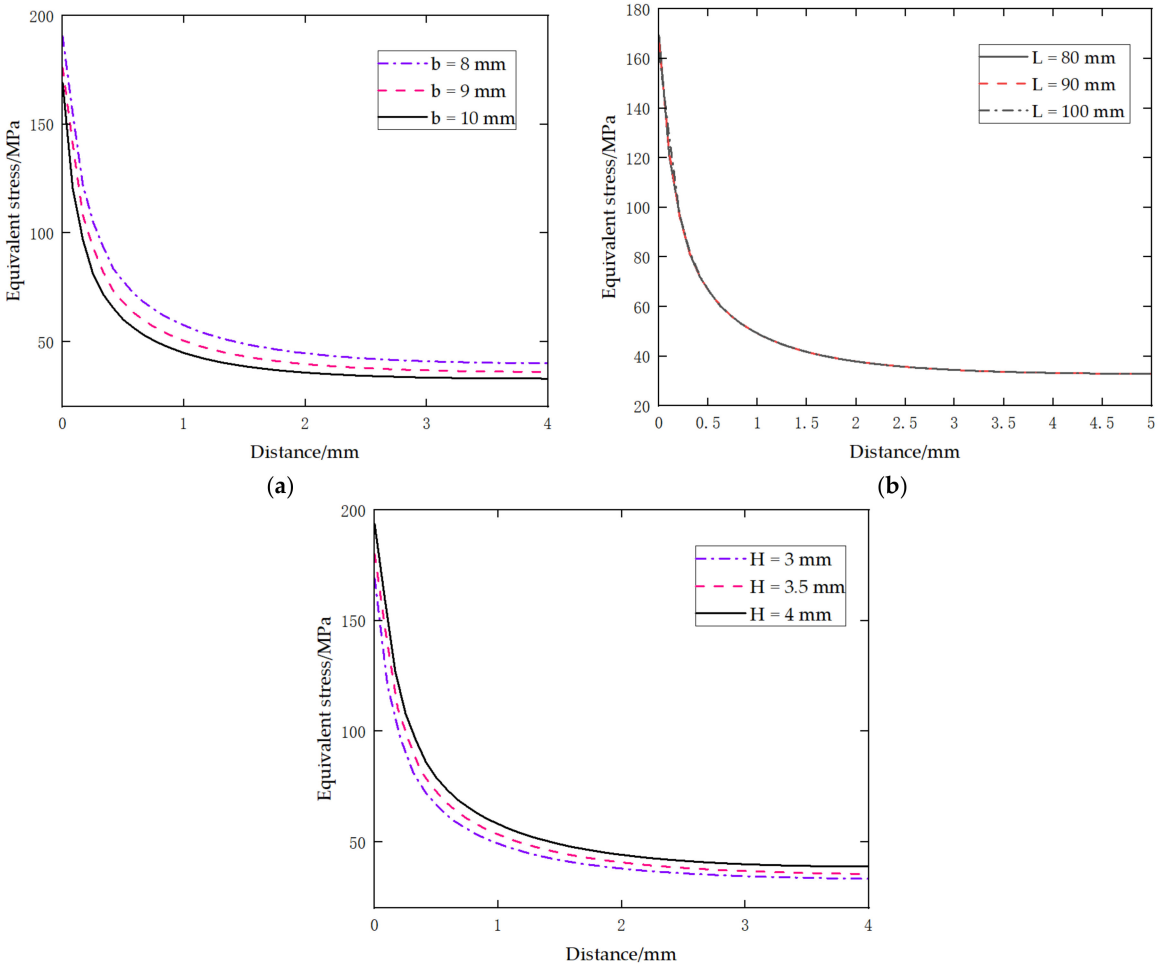

Figure 3. Research results of structural dimensions: (**a**) only change the net width; (**b**) only change the length; (**c**) only change the notch depth.

As can be seen from Figure 3, the stress around the notch decreases as the net width, b, increases and increases as the notch depth, H, increases. The length, L, barely affects the stress field around the notch. Therefore, improvements are made based on Functions (3)~(7). Through a comprehensive analysis of the characteristics of Functions (3)~(5), the ratio of the net width, b, to the notch depth, H, is proposed to replace the constant value before x/R, and then the formula in brackets is uniformly replaced with "$1 + \frac{b}{H} \cdot \frac{x}{R}$". Next, Function (5) is improved, and a new functional expression is proposed, as shown in Function (8).

$$\sigma(x) = \sigma_{\max}\left[a_1 + a_2\left(\frac{R}{R + \frac{b}{H}x}\right) + a_3\left(\frac{R}{R + \frac{b}{H}x}\right)^2 + a_4\left(\frac{R}{R + \frac{b}{H}x}\right)^3\right] \quad (8)$$

Function (8) contains only one design variable—the distance, x, from the bottom of the notch—and b, R, and H are structural parameters.

2.2.2. Verification of the Validity of the Novel Function

To verify the effectiveness and applicability of the new function, semicircular notch, V-notch, and U-notch, which are commonly used in practical engineering, are selected for verification. The length, height, and thickness of the three notched plates are the same, and the notch shape is different. The stress field on the specified path of each notch is first simulated by ANSYS software (American ANSYS, Pittsburgh, PA, USA). Then, the simulated data are fitted with the help of MATLAB (MATLAB R2014a, MathWorks, Natick, MA, USA) using Functions (3)~(8), as shown in Figure 4.

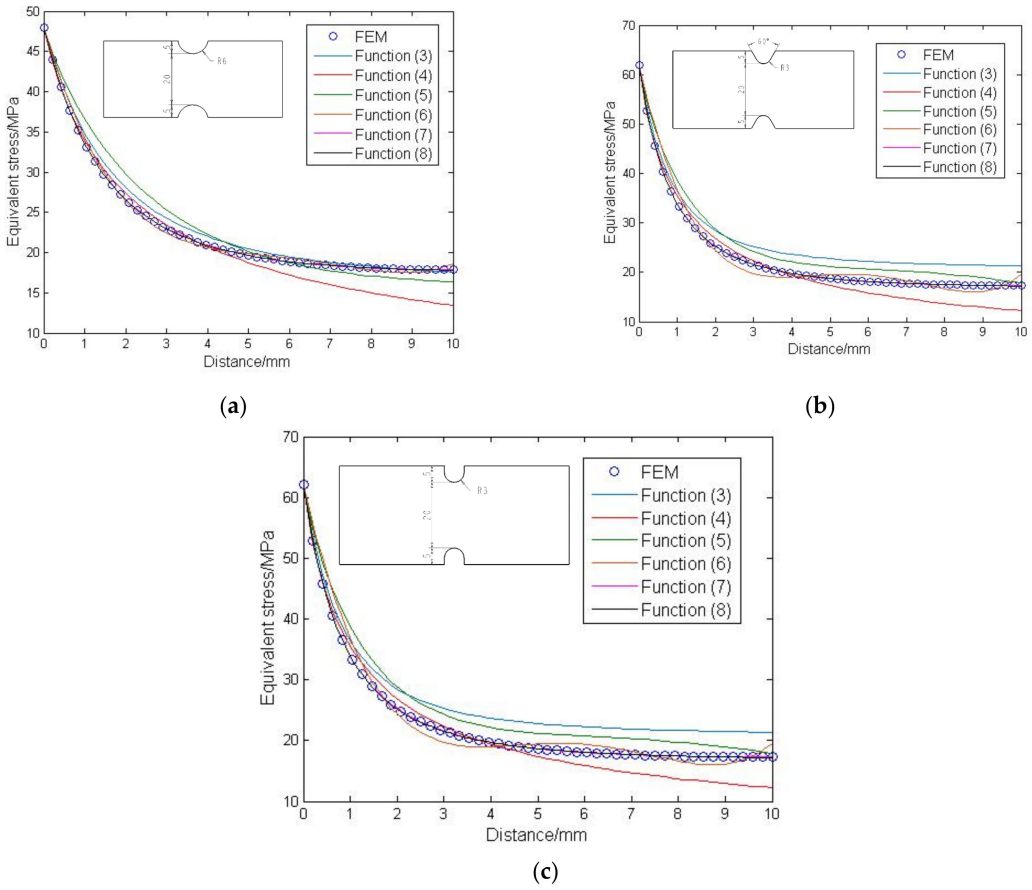

Figure 4. Fitting results of different types of notches: (**a**) semicircular notch; (**b**) V-notch; (**c**) U-notch.

It can be seen from Figure 4 that for different types of notches, Functions (7) and (8) have the best fitting accuracy. To compare the fitting accuracy of Functions (3)~(8), their

R^2 values are calculated separately. R^2 is a statistic that measures how well the regression Equation fits the observations, also known as the determination coefficient, between 0 and 1. The larger the coefficient is, the more accurate the model is and the better the fitting effect is. The definition of R^2 is shown in Equation (9). The R^2 values of each function under different notch types are obtained using MATLAB software (MATLAB R2014a, MathWorks, Natick, MA, USA). The results are shown in Table 1.

$$R^2 = 1 - \frac{\sum_{k=1}^{m} (\widehat{y}_k - y_k)^2}{\sum_{k=1}^{m} (y_k - \overline{y}_k)^2} \tag{9}$$

where m is the number of data points, $\widehat{y}_k$ is the predicted value of the regression model, y_k is the true value, and $\widehat{y}_k$ is the average of all the true values.

Table 1. R^2 value of different types of notches.

Function	Semicircular Notch	V-Notch	U-Notch
Function (3)	0.9850	0.8502	0.8444
Function (4)	0.9160	0.9225	0.9261
Function (5)	0.9200	0.9175	0.9140
Function (6)	0.9967	0.9732	0.9739
Function (7)	0.9992	0.9994	0.9995
Function (8)	0.9996	0.9998	0.9999

From Figure 4 and Table 1, it can be seen that the proposed Function (8) in this paper has the highest fitting accuracy and is commonly applied for all three types of gaps in engineering.

2.2.3. Modification of the Critical Distance

The value of the critical distance is generally determined from the material characteristic length, and the characteristic length is calculated by Equation (10) [38]:

$$L_0 = \frac{1}{\pi}\left(\frac{\Delta K_{th}}{\sigma_0}\right)^2 \tag{10}$$

where ΔK_{th} is the threshold value range of stress intensity factor (unit: MPa·m$^{1/2}$), σ_0 is the fatigue strength of the material (unit: MPa), and L_0 is the material characteristic length (unit: mm).

The traditional critical distance length is often regarded as a material constant; however, this is not the case in practice. Some scholars [19,20] found that the critical distance length is related not only to the material properties but also to the geometric size of the notch. Since the stress concentration factor can best characterize the influence of the geometric size of the notch, it is introduced to modify the traditional critical distance length in this paper. Referring to literature [39], the product of the stress concentration factor and the conventional critical distance is taken as the modified critical distance, and its expression is shown in Equation (11). Compared with the traditional critical distance, the modified critical distance can overcome the notch-size effect in predicting the fatigue limit or fatigue life of notched components so as to obtain more accurate prediction results.

$$\begin{cases} L^*_{PM} = L_0/2 \cdot K_t \\ L^*_{LM} = 2L_0 \cdot K_t \end{cases} \tag{11}$$

where K_t is the stress concentration factor, L^*_{PM} is the modified critical distance in the point method (unit: mm), and L^*_{LM} is the modified critical distance in the line method (unit: mm).

3. Simulation and Experimental Validation

3.1. Prediction of Fatigue Strength of Notched Components with Regular Shape

Based on the new stress Function (8) and the modified critical distance Equation (11), the fatigue strength of a notched component with regular shape is predicted. The selected notched component model is shown in Figure 5, and the dimensions are in mm.

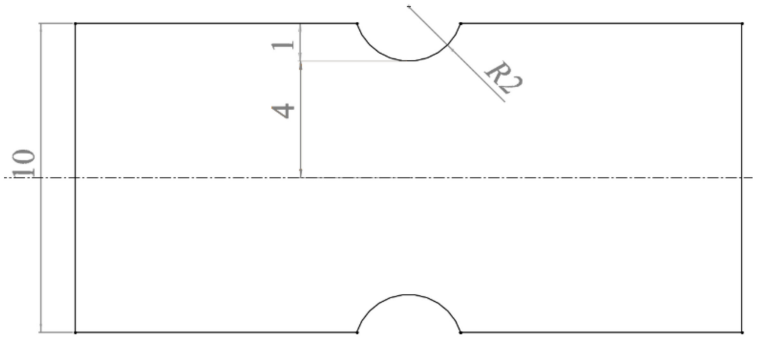

Figure 5. Component with a semicircular notch.

The material of the component with a semicircular notch is Q355, which is the same as the rotating arm. The basic parameters of Q355 are shown in Table 2 [40]. In Table 2, σ_b is the ultimate tensile strength, σ_s is the yield strength, and R_σ is the stress ratio.

Table 2. Basic parameters of Q355.

Material	σ_b (MPa)	σ_s (MPa)	R_σ	ΔK_{th} (MPa·m$^{1/2}$)	σ_0 (MPa)	L_0 (mm)
Q355	500	425	−1	6.36	252	0.203

The critical line method is used to predict the fatigue strength of the notched component. According to the definition of the line method, when fatigue occurs in this notched component:

$$\begin{cases} \frac{1}{L^*_{LM}}\int_0^{L^*_{LM}} \sigma_1(x)dx = \sigma_0 \\ L^*_{LM} = 2L_0 \cdot K_t \\ \sigma_1(x) = K_t\sigma_n[a_1 + a_2(\frac{1}{1+2x}) + a_3(\frac{1}{1+2x})^2 + a_4(\frac{1}{1+2x})^3] \end{cases} \quad (12)$$

where σ_n is the predicted fatigue strength of the component with a semicircular notch, and $\sigma_1(x)$ is the stress function of the component with a semicircular notch.

From Equation (12), the fatigue strength of the component with a semicircular notch can be obtained, as shown in Equation (13).

$$\sigma_n = 2L_0\sigma_0\left[\int_0^{2K_tL_0}(a_1 + a_2(\frac{1}{1+2x}) + a_3(\frac{1}{1+2x})^2 + a_4(\frac{1}{1+2x})^3)dx\right]^{-1} \quad (13)$$

The partial coefficients in Equation (13) are shown in Table 2. The unknown coefficients, K_t and a_1~a_4, are obtained by finite element simulation of the notched component.

Finite element simulation of the above component with a semicircular notch is carried out with the help of ANSYS (American ANSYS, Pittsburgh, PA, USA). First, the finite element model of the component with a semicircular notch is established. Then, the mesh is divided, and loads and constraints are applied. To improve the simulation efficiency, when dividing the mesh, the mesh size of the area close to the notch is smaller, set to 0.2 mm. The mesh size of the part far from the notch can be larger, set to 1 mm. In addition, since the component is mainly subjected to tensile load and the magnitude of the load does not affect the analysis results, a fixed constraint is applied to the left end, and a 1000 N tensile

load is applied to the right end, as shown in Figure 6a. Finally, the stresses on the path from the bottom, point 1 of the notch, to the middle, point 2 of the plate, are analyzed. The specified path is shown in Figure 6b.

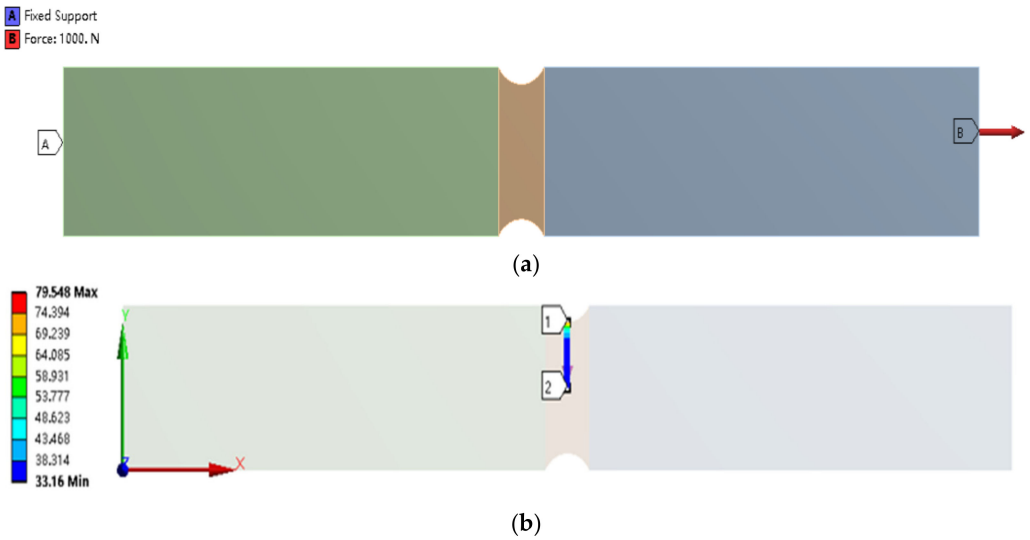

Figure 6. Simulation of the component with a semicircular notch: (**a**) finite element model; (**b**) specified path.

The maximum principal stresses of each point on the specified path are extracted. The results are shown in Table 3.

Table 3. Stress distribution of the specified path.

Node Number	Distance of the Extracted Point (mm)	Maximum Principal Stress (MPa)
1	0	79.55
2	0.20	63.12
3	0.40	52.12
4	0.60	46.76
5	0.80	42.73
6	1.00	40.08
7	1.20	38.21
8	1.40	36.84
9	1.60	35.92
10	1.80	35.19
11	2.00	34.62
12	2.20	34.25
13	2.40	33.89
14	2.60	33.71
15	2.80	33.52
16	3.00	33.40
17	3.20	33.31
18	3.40	33.24
19	3.60	33.20
20	3.80	33.17
21	4.00	33.17

All data in Table 3 are imported into MATLAB (MATLAB R2014a, MathWorks, Natick, MA, USA), and the coefficients a_1~a_4 are obtained, as shown in Table 4.

Table 4. Coefficient value.

a_1	a_2	a_3	a_4
0.2775	−0.1477	1.1768	−0.3068

The stress concentration factor of the component with a semicircular notch is calculated by the finite element method. This value is more accurate than the value obtained by consulting the engineering manual. The definition of stress concentration factor is shown in Equation (14). Through simulation calculation, the stress concentration factor of the component with a semicircular notch is found to be 2.034.

$$\begin{cases} K_t = \sigma_{\max} / \sigma_{nom} \\ \sigma_{nom} = \frac{\int \sigma ds}{s} \end{cases} \tag{14}$$

where σ_{max} and σ_{nom} are the maximum stress and net nominal stress of the notched component, respectively; and s is the length of the integration path.

Substituting all the coefficients into Equation (13), the predicted fatigue strength of the component with a semicircular notch is obtained as:

$$\begin{aligned} \sigma_n &= 2 \times 0.203 \times 252 \left[\int_0^{2 \times 2.034 \times 0.203} (0.2775 - 0.1477 \times (\tfrac{1}{1+2x}) + 1.1768 \times (\tfrac{1}{1+2x})^2 - 0.3068 \times (\tfrac{1}{1+2x})^3) dx \right]^{-1} \\ &= 178 \text{MPa} \end{aligned}$$

To verify the accuracy of the predicted value obtained using the improved TCD, a fatigue test of the component with a semicircular notch is carried out.

3.2. Experimental Verification

Before the fatigue test of the notched specimen, a tensile test of the standard specimen made of the same material is carried out to obtain important properties of the material, mainly including yield strength, tensile strength, and elastic modulus, in preparation for the subsequent fatigue test.

3.2.1. Tensile Test of Standard Specimen

The material of the standard, non-notched specimen is Q355, and the main chemical composition is shown in Table 5.

Table 5. Basic chemical composition of Q355.

Element	C	Si	Mn	P	S	Cr	Ni
Content (%)	0.14	0.25	0.33	0.021	0.007	0.04	0.01

We adopt a rectangular section of the standard specimen, and its geometric dimensions are determined according to ISO 6892-1: 2009 [41]. The specimen dimensions and physical object are shown in Figure 7.

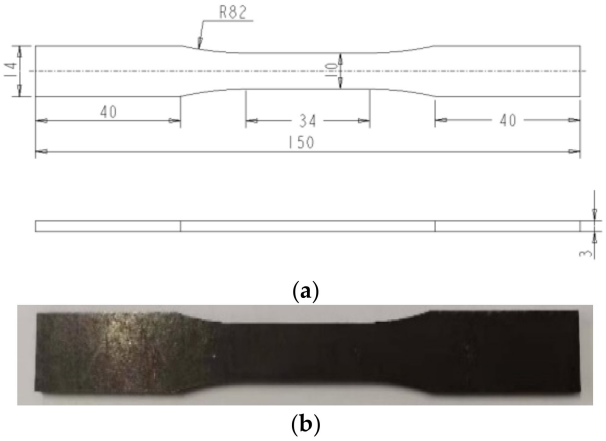

Figure 7. Q355 standard specimen: (**a**) specimen dimensions (unit: mm); (**b**) physical object.

An MTS 370.25 250 kN axial fatigue test system is used for this test, and the test equipment is shown in Figure 8. The testing equipment can carry out the static tensile tests of samples, and the test frequency range is 0~100 Hz. In this paper, the tensile test of the Q355 sample is carried out at room temperature. The displacement control method is adopted, with a stretching speed is 1.2 mm/min and a range of extensometer of 25 mm. To prevent coincidence, three identical specimens are selected for tensile testing.

Figure 8. MTS 370.25.

The tensile fracture of the three specimens is shown in Figure 9. After the test, the load and displacement data of each specimen are collected. The load–displacement curves of the three specimens are obtained according to these test data, and the results are shown in Figure 10. According to the measurement method of relevant parameters [42], the tensile strength, yield strength, and elastic modulus of the three specimens are measured separately from the load–displacement curves. The results are shown in Table 6.

Figure 9. Tensile fracture diagram of specimens.

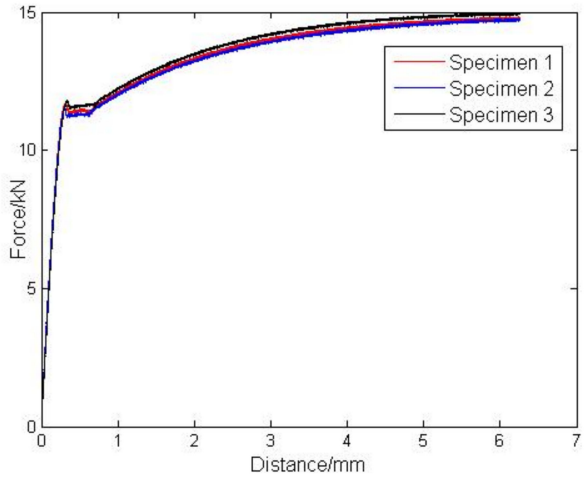

Figure 10. Load–displacement curve of specimens.

Table 6. Mechanical property of Q355.

Specimen Number	σ_b (MPa)	σ_s (MPa)	E (GPa)
1	500	426	206
2	497	422	212
3	503	426	211
Mean value	500	425	210

3.2.2. Fatigue Test of Notched Specimen

The purpose of this fatigue test is to obtain the fatigue strength of the component with a semicircular notch mentioned above and then compare it with the simulation results to verify the effectiveness of the improved TCD. In engineering, the stress corresponding to 10^7 cycles without failure damage under alternating load is generally called the fatigue strength of materials or structures. The common method for measuring the fatigue strength of metal materials or structures is the up-and-down method. Its basic principle is to use the rise and fall of stress to obtain the relevant data under the specified number of cycles, thus calculating the fatigue strength of materials or structures [43].

The geometric dimensions of the notched specimen are determined according to ISO 1099: 2017 [44]. The dimensions and physical object of the notched specimen are shown in Figure 11.

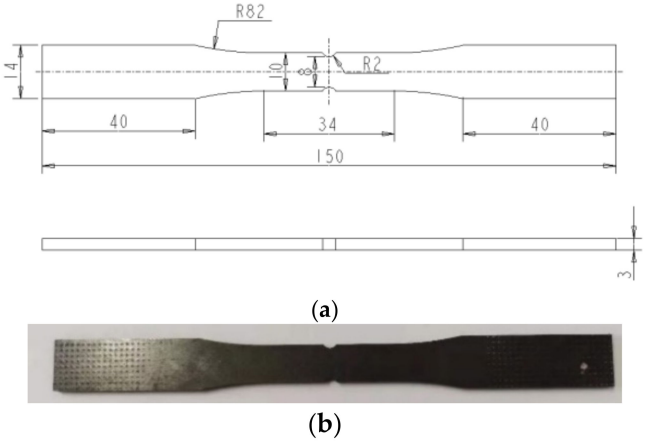

(**a**)

(**b**)

Figure 11. Q355 notched specimen: (**a**) specimen dimensions (unit: mm); (**b**) physical object.

The fatigue test of the notched specimen was carried out on a QBG-100 (Changchun Qianbang Equipment Co., Ltd., Changchun, China) high-frequency fatigue testing machine. The test equipment is shown in Figure 12. The testing machine can carry out static and dynamic load tests. Its maximum load is 500 kN and the maximum loading frequency is 100 Hz. It is found that the number of specimens, stress level difference, and the number of stress levels have an impact on the test results of the up-and-down method [45]. To obtain a more reliable fatigue strength of the Q355 notched specimen, in this paper, the stress levels is controlled at 3~5, and about 16 specimens are selected for the test. At the same time, to avoid the influence of other factors on the test results, all specimens are tested under the same conditions.

Figure 12. QBG-100.

To determine the appropriate initial stress and stress-level difference in this fatigue test, several samples are selected for pretesting. By analyzing the results of pretesting, the first-level stress level of the fatigue test is determined as 0.225 times the tensile strength of Q355, which is 123.75 MPa. The stress level difference is 0.025 times the tensile strength of Q355, which is 13.75 MPa. In addition, in this test, the specified number of cycles, N is, 10^7; the stress ratio, R_σ, is -1; and the experimental frequency, f, is 100 Hz.

After the relevant parameters are determined, the fatigue test of the first specimen is carried out. The test is terminated when the specimen reaches the specified number of cycles or fatigue fracture occurs early. The stress level of the next specimen is determined from the result of the previous specimen. The test steps are the same as those of the first specimen, etc., until six pairs of valid data are collected. During the test, the stress level and the number of cycles of each specimen are recorded.

After the whole fatigue test is completed, the collected data are statistically analyzed. First, all the stress levels in the test are arranged in ascending order, and then all the notched specimens are classified according to the "failure" or "non-failure" event. The classification criteria are as follows: if the number of cycles of a specimen exceeds the specified number of cycles in the test, it is considered a "non-failure" event, indicated by "O", and if the number of cycles is less than the specified number of cycles, it is considered a "failure" event, indicated by "×". Through the above analysis, the up-and-down diagram of the Q355 notched specimen is drawn, as shown in Figure 13.

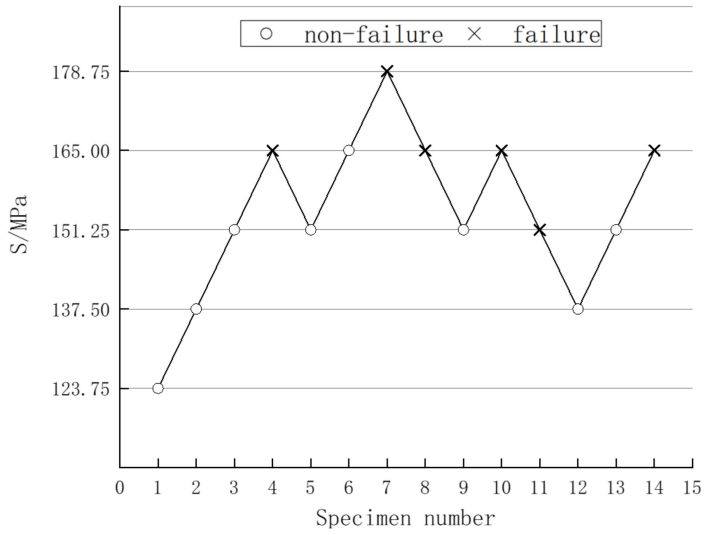

Figure 13. Up-and-down diagram of Q355 notched specimen.

The fatigue strength of the notched specimen is calculated according to Figure 13. Commonly used methods are the mean-value method [46] and the D-M method [47]. The D-M method is a more accurate and simpler method, so in this paper, it is used to calculate the fatigue strength of the notched specimen. The D-M method is based on the principle of maximum likelihood estimation. One of each of the failure events and non-failure events is selected for processing to obtain the fatigue strength of the notched specimen. The fatigue strength is obtained by the following Equation (15):

$$\begin{cases} A = \sum in_i; F = \sum i^2 n_i \\ C = \sum n_i; D = \frac{FC - A^2}{C^2}; \\ S_f = S_1 + d(\frac{A}{C} \pm 0.5) \\ \sigma_f = 1.62d(D + 0.029) \end{cases} \tag{15}$$

where i is the grade of stress level, n_i is the number of specimens at stress level σ_i, S_1 is the lowest stress level, d is the stress level difference, S_f is the mean value of fatigue strength, and σ_f is the standard deviation of fatigue strength.

As can be seen from Figure 13, there are 14 data points in the graph, among which points 1, 2, and 3 are all determined to be non-failure events; points 1 and 2 are omitted; and point 3 is reserved, i.e., there are 12 valid data points. In this test, the data of non-failure events are selected for statistical analysis. It can be seen from Figure 13 that the events involved three stress levels and the statistical results are shown in Table 7.

Table 7. Statistical results of the non-failure event.

Stress Level σ_i (MPa)	Grade i	n_i	in_i	i^2n_i
165.00	3	1	3	9
151.25	2	4	8	16
137.50	1	1	1	1
Sum	-	6	12	26

It can be seen from the data in Table 7 that:

$A = 12$, $F = 26$, $C = 6$, $D = 0.333$, $S_1 = 137.50$, $d = 13.75$

Substituting the above values into Equation (15), the mean value and standard deviation of fatigue strength are obtained, as shown in Equation (16).

$$\begin{cases} S_f = S_1 + d(\frac{A}{C} \pm 0.5) = 172 \text{ MPa} \\ \sigma_f = 1.62d(D + 0.029) = 8.06 \text{ MPa} \end{cases} \tag{16}$$

According to Equation (16), the fatigue strength range of the notched component in Figure 5 is (163.94, 180.06). The predicted fatigue strength using the improved TCD in Section 3.1 is 178 MPa, which is within the above range, indicating that TCD is improved effectively in this paper.

3.2.3. Results Analysis

In this paper, improvements are made in the stress function and critical distance of the classic TCD. To verify the reliability and accuracy of the improved TCD, the results obtained based on the improved TCD, the classic TCD, and the fatigue test are compared. The results are shown in Table 8.

Table 8. Comparison of results.

	Experimental Mean Value	Classic TCD	Improved TCD		
			Only Improved Stress Function	Only Improved Critical Distance Value	Both
Fatigue Strength (MPa)	172	154.60	154.27	179.05	178
Error	-	10%	10%	4%	3.5%

As can be seen from Table 8, comparing the classic TCD with the improved TCD, which only improves the stress function, it is found that the difference between the two prediction results is very small. This indicates that the new stress function can describe the stress field near the notch as accurately as the commonly used fourth-order stress function, whereas the lower order of the new function makes its calculation less accurate. In addition, comparing the result of the classic TCD with that of the improved TCD, which only changes the critical distance, it is found that the change of the critical distance has a greater influence on the predicted value of fatigue strength. In this paper, the modification for the critical distance makes the prediction result closer to the experimental value. The result obtained by simultaneously improving stress function and critical distance is compared with the results obtained by other methods, and it is found that the former has the smallest error compared to the experimental value. Therefore, the novel stress function and the modified critical distance can be used to accurately predict the fatigue performance of notched components.

The rotating arm is the primary force member of the turning mechanism and is most susceptible to fatigue damage in practice. Therefore, fatigue life analysis is carried out for the rotating arm.

4. Fatigue Life Prediction of the Rotating Arm Based on Improved TCD

TCD can be used to predict the fatigue strength and fatigue life of notched components. In the previous section, the fatigue strength of a notched part was predicted and experimentally verified, with the aim of verifying the effectiveness of the improved TCD. In this section, the improved TCD is applied to engineering practice. This improved TCD method is used to predict the fatigue life of a turning mechanism. Through comparison with the test life, the accuracy of the improved TCD is once again verified.

The turning mechanism consists of a driving cylinder, rotating arm, pulling arm, turning frame, and pressing mechanism [4], as shown in Figure 14. The working principle of the turning mechanism is to lift and turn the trash can so that the rubbish is dumped into the carriage. The trajectories of the trash can are shown in Figure 15. During operation, the rotating arm is the central part of the turning mechanism. The rotating arm is irregular in shape and most susceptible to fatigue damage at the notch; therefore, the fatigue life of the rotating arm is investigated using the improved TCD.

Figure 14. Turning mechanism.

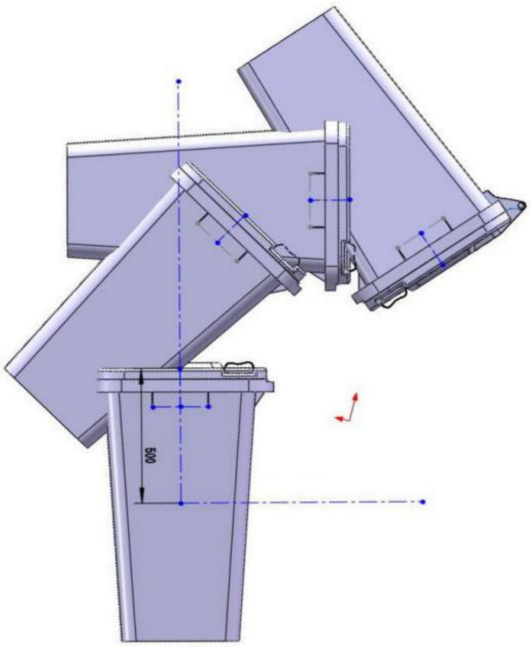

Figure 15. Trajectories of the trash can.

4.1. Establishment of Finite Element Model and Stress Analysis

Simulation of the rotating arm component is carried out with the help of ANSYS (American ANSYS, Pittsburgh, PA, USA). The three-dimensional model of the rotating arm under maximum force conditions is first established, and then the equivalent stress cloud of the rotating arm is obtained by dividing the mesh and applying load constraints. The load constraint of the rotating arm is obtained by dynamics simulation. The hinge hole on the right is connected with the carriage and set as a fixed constraint. The upper hinge hole is connected with the turning frame, and the forces in X direction and Y direction are 2437 N and −12.548 N, respectively. The hinge hole on the left is connected with the driving cylinder, and the forces in X direction and Y direction are −24582 N and 9116 N, respectively, as shown in Figure 16a. In addition, the mesh type hexahedral with a size of 2 mm.

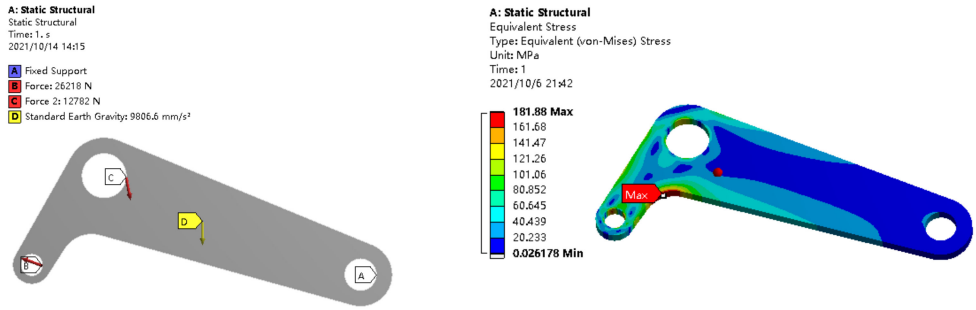

(**a**) (**b**)

Figure 16. Static simulation analysis of the rotating arm: (**a**) applying loads and constraints; (**b**) equivalent stress cloud chart.

As shown in Figure 16b, the maximum equivalent stress of the rotating arm occurs at the lower arc, with a magnitude of 181.88 MPa, and the position is also most prone to fatigue damage in practice.

4.2. Calculation of the Rotating Arm Effective Stress

The difficulty in applying TCD to irregularly shaped components lies mainly in the determination of the focusing path. The focusing path is the direction of the highest stress gradient, which needs to be explored for the rotating arm, as there is little relevant research available. According to the relevant literature [31], in this paper, we assume that the direction of the focus path of the rotating arm is the direction of the angle bisector of the arc where the maximum stress is located. The following attempts are made to verify the above assumptions:

(1) Determine the coordinates of the point of maximum stress in the rotating arm, then draw a circle with that point as the center and a radius of 30 mm.
(2) Select the directions 0°, 20°, 40°, 60°, −20°, −40°, and −60° in the circumferential direction and draw the corresponding stress–distance curves, as shown in Figure 17.

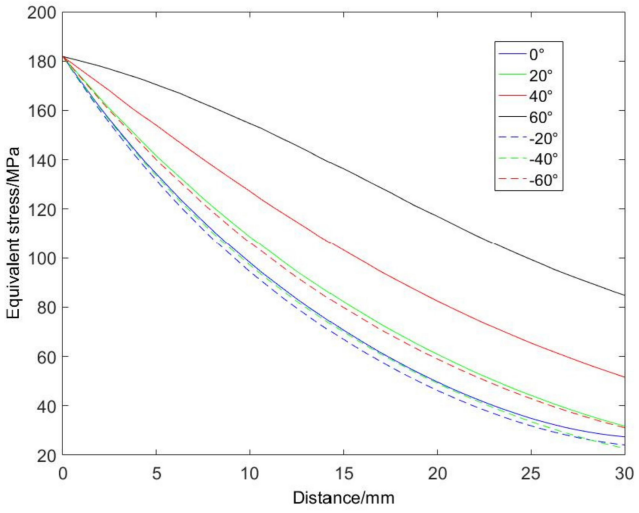

Figure 17. Stress–distance curve of each path.

Figure 17 shows that the stresses change fastest in the −20° direction, which is the direction of the circular arc angle bisector, proving the above hypothesis. The stresses in this direction are extracted from the rotating arm and fitted using Function (8) to obtain the stress-fitting Function (17). The resulting fitted curve is compared with the finite element simulation and found to be a good fit, as shown in Figure 18.

$$\sigma_{Eq}(x) = 181.88 \times \left[5.67 - 18.21 \times \left(\frac{50}{50+0.6x}\right) + 17.26 \times \left(\frac{50}{50+0.6x}\right)^2 - 3.71 \times \left(\frac{50}{50+0.6x}\right)^3\right] \quad (17)$$

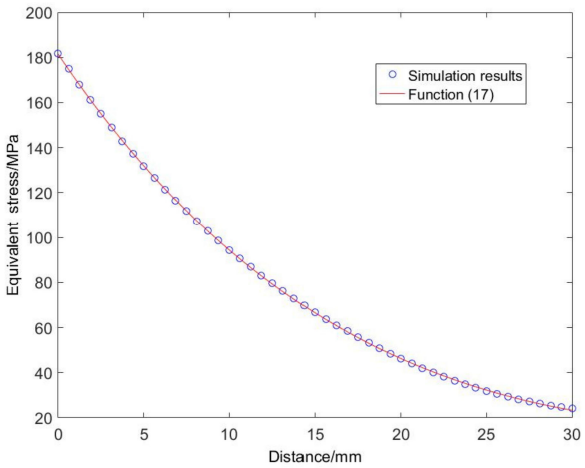

Figure 18. Stress distribution curve on focusing path.

After the stress function of the rotating arm is determined, its critical distance value is calculated. In this paper, the material of the rotating arm is Q355 steel. According to the relevant literature [40], the fatigue limit of Q355 at stress a ratio R = 0 is 231 MPa and the threshold value of the stress intensity factor is 6.57 MPa·m$^{1/2}$. By substituting the above values into Equation (10), the characteristic length is obtained as 0.257 mm. The stress concentration factor is calculated by the finite element method, which is more accurate than the value obtained by consulting the engineering manual. Based on the definition of the stress concentration factor and the simulation results of the rotating arm, the stress concentration factor of the rotating arm is calculated as 2.42. The critical distance of the rotating arm is obtained as 1.244 mm by substituting the characteristic length and the stress concentration factor into the modified critical distance Equation (11). The critical distance value obtained by the above method generally corresponds to 10^7 cycles, which is an infinite life. However, the life of the rotating arm is finite. In this case, the critical distance value should increase with the reduction in the number of cycles. However, through analysis of the rotating arm structure, it is found that when the integral region reaches the modified critical distance value of 1.244 mm, the effective stress tends to be stable, and the region after 1.244 mm has little effect on the effective stress. Therefore, in this paper, we select the modified critical distance value to calculate the effective stress of the rotating arm so as to estimate the finite life of the rotating arm.

The effective stress of the rotating arm is calculated based on the critical line method, which can be obtained according to the definition of the line method. The effective stress of the rotating arm can be obtained by substituting the critical distance and stress function of the rotating arm obtained earlier into Equation (18).

$$\sigma_{eff1} = \frac{1}{L}\int_0^L \sigma_{Eq}(x)dx \quad (18)$$

In the above process of calculating the effective stress of the rotating arm, the size factor and surface-quality factor are not included. However, in practice, these factors also affect the fatigue life of the rotating arm. Therefore, this aspect is covered in the following section.

4.3. Establishment of S–N Curve

The S–N curve is generally expressed in logarithmic form, namely:

$$\log N = a + b \log S \tag{19}$$

where N is the Number of cycles, S is the stress amplitude, and a and b are material constants.

The material of the rotating arm is Q355. First, it is necessary to obtain the S–N curve of Q355. By reviewing the relevant literature [48], the S–N curve of Q355 at room temperature is obtained, as shown in Equation (20).

$$\log N = 34.57 - 11.48 \log S \tag{20}$$

However, the S–N curve of Q355 is generally measured under ideal conditions, which is very different from attainment of the real S–N curve of the rotating arm. Therefore, in order to obtain the S–N curve of the rotating arm, Equation (20) needs to be modified. According to the previous analysis, the maximum stress of the rotating arm is far less than its yield strength is considered high-cycle fatigue. Therefore, $N = 10^3$ and $N = 10^7$ are taken as the starting and ending point, respectively, of the modified S–N curve. When the coordinates of the two points (S'_{10^3}, 10^3) and (S'_f, 10^7) are determined, the expressions of the modified S–N curve can be obtained.

First, the fatigue limit value at $N = 10^7$ is corrected; the expression of the corrected fatigue limit value is shown in Equation (21).

$$S'_f = \frac{S_f}{K_f} \varepsilon \cdot \beta \cdot C_L \tag{21}$$

where S'_f is the modified fatigue limit, S_f is the fatigue limit of the standard specimen, K_f is the fatigue notch factor, ε is the size factor, β is the surface quality factor, and C_L is the load factor.

According to the actual situation of the rotating arm, the above coefficients can be obtained by consulting the mechanical design manual and are as follows [40]:

$\varepsilon = 0.79$, $\beta = 0.84$, $C_L = 0.85$, $K_f = 2$

Substituting the above coefficient values into Equation (21), the modified fatigue limit value, S'_f, is obtained as 70.56 MPa.

Next, the stress value at $N = 10^3$ is corrected; the expression of the corrected stress value is shown in Equation (22).

$$S'_{10^3} = \frac{S_{10^3}}{K_f} \cdot \varepsilon \cdot \beta \cdot C_L \tag{22}$$

where S_{10^3} is the stress value of the S–N curve of Q355 at $N = 10^3$.

According to the above analysis, the coordinates of the two modified points are (159.65, 10^3) and (70.56, 10^7). Substituting them into Equation (19), the S–N curve of the rotating arm is obtained, as shown in Equation (23).

$$\log N = 28.20 - 11.28 \log S \tag{23}$$

4.4. Analysis of Fatigue Life Prediction Results

In practice, the rotating arm is mainly subjected to tensile load during the lifting process. When all the garbage is dumped, the rotating arm returns with no load, and there is almost no force in this process. It can be considered that the force on the rotating arm is 0 during the return process. The load variation of the rotating arm in one cycle approximately satisfies the sinusoidal curve. The rotating arm is mainly subjected to tensile load during whole operation; the average stress is not zero, so the Goodman formula is

used to correct the average stress of the rotating arm. The Goodman formula is shown in Equation (24) [49]:

$$\frac{\sigma_a}{\sigma_{-1}} + \frac{\sigma_m}{\sigma_b} = 1 \tag{24}$$

where σ_a is the stress amplitude, σ_m is the average stress, σ_{-1} is the fatigue strength under symmetrical cyclic loading, and σ_b is the ultimate tensile strength.

The fatigue life of the turning mechanism is predicted using the modified TCD. According to the definition of TCD, the effective stress of the turning arm is determined to be 175 MPa. Since this value is obtained based on the most dangerous working condition of the turning arm, the maximum stress of the turning arm in one cycle can be considered to be 175 MPa and the minimum stress to be 0. Thus, the cyclic load spectrum of the turning arm is obtained, as shown in Figure 19a, by inputting the load spectrum, S–N curve, and Goodman formula of the rotating arm in the MSC. Using fatigue software, the fatigue life of the rotating arm is calculated to be 282,580 cycles.

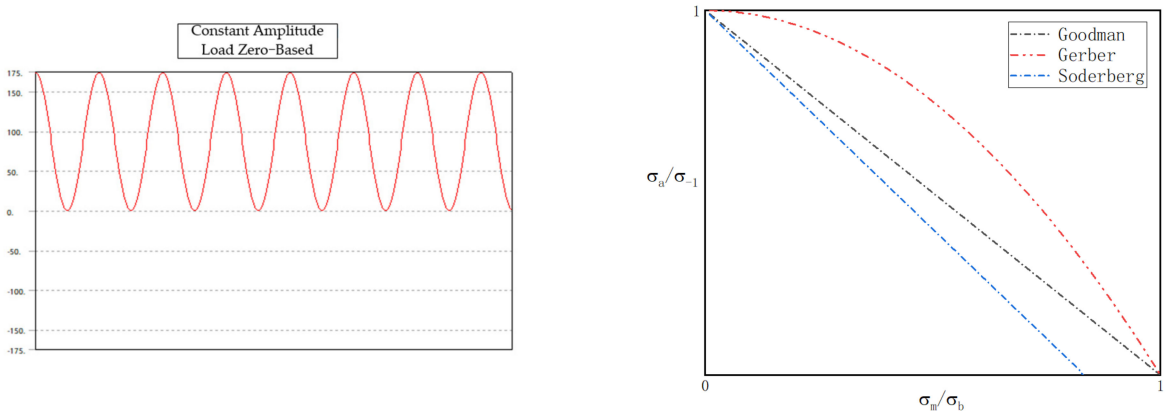

(**a**) (**b**)

Figure 19. Sinusoidal load spectrum of the rotating arm: (**a**) sinusoidal load spectrum; (**b**) Goodman formula.

In the past, the nominal stress method was often used to analyze the fatigue life of turnover mechanisms. This method takes the nominal stress of the structure as the control parameter, and the analysis process is similar to that of TCD. By setting the nominal stress spectrum, the S–N curve, and the Goodman formula of the rotating arm, the fatigue life of the rotating arm is calculated to be 167,850 cycles, as shown in Figure 20.

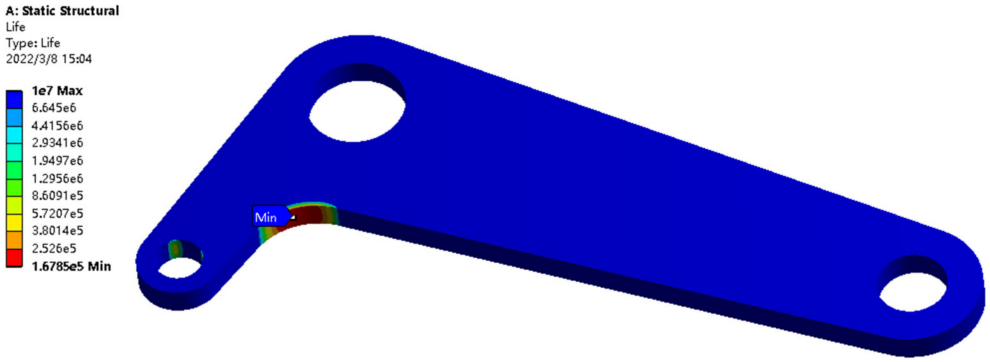

Figure 20. Fatigue life cloud diagram of rotating arm based on the nominal stress method.

The manufacturer of this model of garbage truck has carried out fatigue experiments on the turning mechanism, and the experimental life obtained under the same conditions is

240,000 cycles. A comparison of the fatigue life acquired by the three methods is shown in Table 9.

Table 9. Comparison of fatigue life results.

	Experimental Life	Nominal Stress Method	Improved TCD
Fatigue life (cycle)	240,000	167,850	282,580
Error	-	30%	18%

As shown in Table 9, the fatigue life calculated based on the nominal method is more conservative, and the fatigue life predicted by the improved TCD method is higher. However, although the improved TCD method overestimates the fatigue life of the turning mechanism, its error concerning test life is smaller, which shows that the improved TCD proposed in this paper can be used for fatigue life analysis of key components of turning mechanisms.

5. Conclusions

The purpose of this paper is to propose an improved TCD method to accurately predict the fatigue life of key components of the turning mechanism in garbage compression trucks. The main conclusions reached are as follows:

(1) The traditional theory of critical distances is improved in terms of both the stress function and the critical distance length. By analyzing the influence mechanism of the crucial dimensional parameters of the structure on the stress, a high-computational-efficiency and high-accuracy stress function is proposed by introducing the notch depth and net width into the traditional function. In addition, in this paper, we introduce a stress concentration factor to modify the critical distance length.

(2) To verify the effectiveness of the improved TCD, a notched component with regular shape is selected for fatigue strength prediction. In addition, fatigue a test is carried out on the notched component. The error between the predicted and tested value is found to be 3.5%, indicating that the improved TCD in this paper is accurate and applicable to the fatigue study of notched components with regular shapes.

(3) To accurately predict the fatigue life of key components of turning mechanisms with irregular shapes, the improved TCD method is used for fatigue life analysis. In comparison with existing test results, it is found that the improved TCD method has a higher prediction accuracy than the nominal stress method. This shows that the improved TCD can be used for fatigue life prediction of key components of turning mechanisms and provide a theoretical basis for fatigue life study of other notched components with irregular shapes in engineering.

Author Contributions: Methodology, H.Z.; software, H.Z.; validation, T.W. and H.Z.; formal analysis, D.Q.; writing—original draft preparation, H.Z.; writing—review and editing, T.W. and M.W.; visualization, T.W. and Y.D.; supervision, D.Q.; project administration, T.W.; funding acquisition, T.W. All authors have read and agreed to the published version of the manuscript.

Funding: This research was funded by the National Natural Science Foundation of China—Research on integrated design method of structure-material-performance of automobile body based on big data (51705468)—and the Key Technologies Research and Development Program—Research on key technologies for lightweight of whole vehicles (2018YFB0106204-03).

Institutional Review Board Statement: Our research does not involve humans or animals.

Informed Consent Statement: This article does not involve the study of humans.

Data Availability Statement: The research does not report any data, and we have chosen to exclude this statement.

Conflicts of Interest: The authors declare no conflict of interest.

References

1. Kim, J.-S. Fatigue assessment of tilting bogie frame for Korean tilting train: Analysis and static tests. *Eng. Fail. Anal.* **2006**, *13*, 1326–1337. [CrossRef]
2. Baek, S.H.; Cho, S.S.; Joo, W.S. Fatigue life prediction based on the rainflow cycle counting method for the end beam of a freight car bogie. *Int. J. Automot. Technol.* **2008**, *9*, 95–101. [CrossRef]
3. Yang, B.; Duan, H.; Wu, S.; Kang, G. Damage Tolerance Assessment of a Brake Unit Bracket for High-Speed Railway Welded Bogie Frames. *Chin. J. Mech. Eng.* **2019**, *32*, 58. [CrossRef]
4. Ge, X. Fatigue Life Analysis of Lifting Mechanism Based on Finite Element and Multi-Body Dynamics. Master's Thesis, Qingdao University, Shandong, China, 2014.
5. Qian, Z. Design and Research of the Executing Mechanism of Side Packed Compression Garbage Truck. Master's Thesis, Shandong University of Science and Technology, Shandong, China, 2017.
6. Neuber, H. *Theory of Notch Stresses: Principles for Exact Calculation of Strength with Reference to Structural Form and Material*, 2nd ed.; Springer: Berlin/Heidelberg, Germany, 1958.
7. Peterson, R.E. Notch sensitivity. In *Metal Fatigue*; McGraw Hill: New York, NY, USA, 1959; pp. 293–306.
8. Clegg, R.; Duan, K.; McLeod, A.J. The theory of critical distances and fatigue from notches in aluminium 6061. *Fatigue Fract. Eng. Mater. Struct.* **2012**, *35*, 13–21. [CrossRef]
9. Louks, R.; Susmel, L. The linear-elastic Theory of Critical Distances to estimate high-cycle fatigue strength of notched metallic materials at elevated temperatures. *Fatigue Fract. Eng. Mater. Struct.* **2015**, *38*, 629–640. [CrossRef]
10. Cheng, Z.; Liao, R.; Lu, W.; Wang, D. Fatigue notch factors prediction of rough specimen by the theory of critical distance. *Int. J. Fatigue* **2017**, *104*, 195–205. [CrossRef]
11. Spaggiari, A.; Castagnetti, D.; Dragoni, E.; Bulleri, S. Fatigue life prediction of notched components: A comparison between the theory of critical distance and the classical stress-gradient approach. *Procedia Eng.* **2011**, *10*, 2755–2767. [CrossRef]
12. Zamzami, A.l.; Susmel, L. On the accuracy of nominal, structural, and local stress based approaches in designing aluminium welded joints against fatigue. *Int. J. Fatigue* **2017**, *101*, 137–158. [CrossRef]
13. Zheng, H.; Filippo, B.; Youshi, H. Comparison of TCD and SED methods in fatigue lifetime assessment. *Int. J. Fatigue* **2019**, *123*, 105–134.
14. Glinka, G.; Newport, A. Universal features of elastic notch-tip stress fields. *Int. J. Fatigue* **1987**, *9*, 143–150. [CrossRef]
15. Kujawski, D.; Shin, C. On the elastic longitudinal stress estimation in the neighbourhood of notches. *Eng. Fract. Mech.* **1997**, *56*, 137–138. [CrossRef]
16. Filippi, S.; Lazzarin, P.; Tovo, R. Developments of some explicit formulas useful to describe elastic stress fields ahead of notches in plates. *Int. J. Solids Struct.* **2002**, *39*, 4543–4565. [CrossRef]
17. Huang, N. Research on Fatigue Life Prediction Methods for Large-Scale Components. Master's Thesis, Central South University, Changsha, China, 2013.
18. Sun, D.; Hu, Z. Research of the Size Factor of Fatigue Strength Base on TCD Theory. *Chin. Quart. Mech.* **2015**, *36*, 288–295.
19. Lanning, D.B.; Nicholas, T.; Haritos, G.K. On the use of critical distance theories for the prediction of the high cycle fatigue limit stress in notched Ti-6Al-4V. *Int. J. Fatigue* **2005**, *27*, 45–57. [CrossRef]
20. Yamashita, Y.; Ueda, Y.; Kuroki, H.; Shinozaki, M. Fatigue life prediction of small notched Ti–6Al–4V specimens using critical distance. *Eng. Fract. Mech.* **2010**, *77*, 1439–1453. [CrossRef]
21. Taddesse, A.T.; Zhu, S.-P.; Liao, D.; Huang, H.-Z. Cyclic plastic zone modified critical distance theory for notch fatigue analysis of metals. *Eng. Fail. Anal.* **2021**, *121*, 105163. [CrossRef]
22. Yang, X.; Wang, J.; Liu, J. High temperature LCF life prediction of notched DS Ni-based superalloy using critical distance concept. *Int. J. Fatigue* **2011**, *33*, 1470–1476. [CrossRef]
23. Wang, R.; Li, D.; Hu, D.; Meng, F.; Liu, H.; Ma, Q. A combined critical distance and highly-stressed-volume model to evaluate the statistical size effect of the stress concentrator on low cycle fatigue of TA19 plate. *Int. J. Fatigue* **2017**, *95*, 8–17. [CrossRef]
24. Sun, S.; Yu, X.; Liu, Z.; Chen, X. Component HCF Research Based on the Theory of Critical Distance and a Relative Stress Gradient Modification. *PLoS ONE* **2016**, *11*, e0167722. [CrossRef]
25. Moritz, B.; André, M.M.; Aleksandar-Saša, M. Requirements for stress gradient-based fatigue assessment of notched structures according to theory of critical distances. *Fatigue Fract. Eng. Mater. Struct.* **2020**, *7*, 1541–1554.
26. Shen, J.; Fan, H.; Wang, J.; Yu, C.; Huang, Z. A fatigue life evaluation method for notched geometries considered the stress gradient concept. *Int. J. Fract.* **2021**, 1–16. [CrossRef]
27. Wang, R.; Liu, H.; Hu, D.; Li, D.; Mao, J. Evaluation of notch size effect on LCF life of TA19 specimens based on the stress gradient modified critical distance method. *Fatigue Fract. Eng. Mater. Struct.* **2018**, *41*, 1794–1809. [CrossRef]
28. Li, Z.; Shi, D.; Li, S.; Yang, X.; Miao, G. A systematical weight function modified critical distance method to estimate the creep-fatigue life of geometrically different structures. *Int. J. Fatigue* **2019**, *126*, 6–19. [CrossRef]
29. Susmel, L.; Taylor, D. A simplified approach to apply the theory of critical distances to notched components under torsional fatigue loading. *Int. J. Fatigue* **2006**, *28*, 417–430. [CrossRef]
30. Susmel, L.; Taylor, D. A critical distance/plane method to estimate finite life of notched components under variable amplitude uniaxial/multiaxial fatigue loading. *Int. J. Fatigue* **2012**, *38*, 7–24. [CrossRef]

31. Liu, B.; Yan, X. An extension research on the theory of critical distances for multiaxial notch fatigue finite life prediction. *Int. J. Fatigue* **2018**, *117*, 217–229. [CrossRef]
32. Benedetti, M.; Fontanari, V.; Allahkarami, M.; Hanan, J.; Bandini, M. On the combination of the critical distance theory with a multiaxial fatigue criterion for predicting the fatigue strength of notched and plain shot-peened parts. *Int. J. Fatigue* **2016**, *93*, 133–147. [CrossRef]
33. Nicholas, G.; Fatemi, A. Multiaxial variable amplitude fatigue life analysis including notch effects. *Int. J. Fatigue* **2016**, *91*, 337–351.
34. Liu, Z.; Correia, J.; Carvalho, H. Global-local fatigue assessment of an ancient riveted metallic bridge based on submodelling of the critical detail. *Fatigue Fract. Eng. Mater. Struct.* **2019**, *42*, 546–560. [CrossRef]
35. Horas, C.S.; Correia, J.; Jesus, A.D. Application of Modal Superposition Technique in the Fatigue Analysis Using Local Approaches. *Procedia Eng.* **2016**, *160*, 45–52. [CrossRef]
36. Liu, Y.; Deng, C.; Gong, B. Discussion on equivalence of the theory of critical distances and the coupled stress and energy criterion for fatigue strength prediction of notched specimens. *Int. J. Fatigue* **2020**, *131*, 105326. [CrossRef]
37. Xu, R.X.; Thompson, J.C.; Topper, T.H. Practical stress expressions for stress concentration regions. *Fatigue Fract. Eng. Mater. Struct.* **1995**, *18*, 885–895. [CrossRef]
38. Sánchez, M.; Cicero, S.; Arroyo, B.; Álvarez, J.A. Coupling Finite Element Analysis and the Theory of Critical Distances to Estimate Critical Loads in Al6060-T66 Tubular Beams Containing Notches. *Metals* **2020**, *10*, 1395. [CrossRef]
39. Wang, J.; Yang, X. HCF strength estimation of notched Ti–6Al–4V specimens considering the critical distance size effect. *Int. J. Fatigue* **2012**, *40*, 97–104. [CrossRef]
40. Wen, B. *Mechanical Design Manual: Fatigue Strength and Reliability Design*; China Machine Press: Beijing, China, 2015.
41. *ISO 6892-1: 2009*; Metallic Materials—Tensile Test Method—Part 1: Method of Test at Room Temperature. ISO: Geneva, Switzerland, 2009.
42. Zhang, C.; Jin, H.; Zhu, L. Experimental research on fatigue properties of Q345 steel after natural cooling down from high temperature. *J. Build. Struct.* **2020**, *41*, 78–85.
43. He, X.; Xie, W. Several Test Methods of Fatigue Limits of Metalic Materials. *Phys. Tes Anal.* **2015**, *51*, 388–393.
44. *ISO 1099: 2017*; Metallic Materials—Fatigue Testing—Axial Force-Controlled Method. ISO: Geneva, Switzerland, 2017.
45. Kai, L.; Jiang, Q.; Wang, F. Cause of error in average and standard deviation of fatigue strength measured by up-and-down method. *Phys. Tes Anal.* **2021**, *57*, 7–13.
46. Gao, Z. *Fatigue Applied Statistics*; National Defense Industry Press: Beijing, China, 1986.
47. Li, R. Test study on fatigue property of thin steel sheet for automobile. Master's Thesis, Dalian University of Technology, Dalian, China, 2012.
48. Jia, D.; Liao, X.; Cui, J. Experimental Study on High Cycle Fatigue Behavior and γ-P-S-N Curves of Bridge Steel Q345qD. *J. TJ. Univer.* **2016**, *49*, 122–128.
49. Yong, L.; An, Z.; Bo, L. Fatigue life prediction for wind turbine main shaft bearings. In Proceedings of the International Conference on Quality, Reliability, Risk, Maintenance, and Safety Engineering (QR2MSE), Chengdu, China, 15–17 July 2013.